The relevant scale for mechanical modelling in additive manufacturing technologies

Sofiane Guessasma [1], Sofiane Belhabib[2]
1. INRA, rue de la géraudière, 44316 Nantes, France
2. GEPEA, UMR CNRS 6144, , IUT of Carquefou, 2 avenue du Pr. Jean Rouxel, 44475 Carquefou Cedex, France

Introduction

Additive manufacturing (AM) is a new way of manufacturing complex three-dimensional objects from digital models[1]. A large number of processes are associated with the AM technologies such as fused deposition modeling, inkjet and stereolithography. These technologies share, however, the same principle of building layer by layer in an additive way the material where needed in the three dimensional space [2]. The main advantage of AM technologies over classical approaches such as injection molding is the weak dependence on tooling that allows AM to provide a short fabrication cycle (i.e., number of unit steps to accomplish the realization of a technical part) with a higher degree of freedom in the design of complex and personalized items[3]. We see nowadays many of the key industries such as biomedical, aerospace, automotive, construction, and food industry that have already embraced such manufacturing technique for different applications [4-8]. FDM that stands for Fused Deposition Modelling is among these popular AM technologies based on the laying down of fused filaments. These filaments come in the form of wires of 1 to 3 mm in diameter and are heated then extruded in smaller filaments of typical 100 µm in diameter[9]. FDM has been used so far successfully to process polymeric structures [10-12]. Because of the nature of one dimensional laying down process, material discontinuities within the printed structures are observed. These discontinuities induce a loss of mechanical performance in addition to the lack of cohesion between filaments that are widely reported in the literature [13-15].

This study aims at revealing the role of microstructural defects as driving factors for the mechanical performance of polymeric parts designed using FDM. Structural mechanics module from Comsol software is used to predict the compression performance of 3D printed polymeric structures. Assuming a plane strain loading state, geometries of 3D prints are modelled as 2D plans using various forms of filament arrangements representing the effect of raster angle in FDM. 3D prints are considered as full dense materials. The constitutive laws are implemented in a way to authorize the lack of adhesion between adjacent filaments and to induce damage depending on the load level. Simulation of severe compression levels is considered and the stress fields are analyzed. Comparison between the experimental and numerical performance is discussed based on mechanical testing and X-ray micro-tomography imaging.

Experimental Set-up

The polymer ABS (Acrylonitrile Butadiene Styrene) is used as a feedstock material. This polymer is purchased from CADvision company (Guyancourt, France) under the reference P430XL ABS in the form of wires of 1.75 mm in diameter. The geometry considered is a cube of 30 mm in size. This simple CAD model is printed using uPrint SE 3D printer from Stratasys. The printing process is conducted with a resolution of 254 µm. During the printing process, dissolvable support is needed only in the first layers between the part and the print bed. The software CatalystEX is used to convert the CAD model into stl file then to series of toolpaths. The printing angle θ is the main variable in this study (Figure 1).
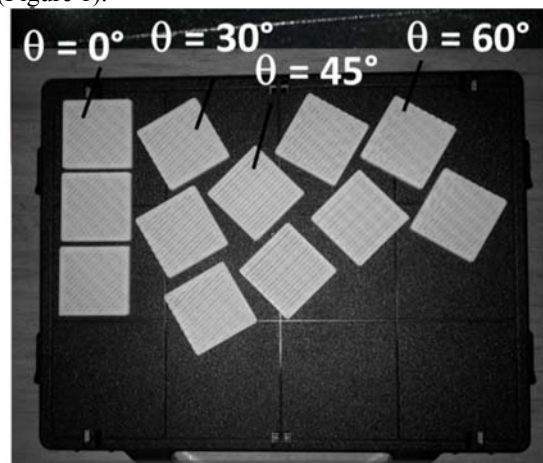

Figure 1. Printing configurations considered in this study. The printing angle θ is varied from 0° to 60°.

Four different values are selected, namely 0°, 30°, 45°, and 60° allowing for filaments to be crossed within the plane of deposition in different sequences (-45°/+45°), (-15°/+75°),(-0°/+90°),(+15°/-75°).

Uniaxial compression is performed on the main directions of the cubes X, Y and Z directions using a universal machine (100 KN MTS machine) under a constant load rate of 10mm/min. Up to 60% of reduction in height is considered to induce a severe compression condition (Figure 2).

Figure 2. Testing setup comprising high speed camera observation and universal testing machine.

The microstructures of 3D printed cubes before and after loading are imaged using X-ray micro-tomography (UltraTom X-ray µ-CT system). This technique allows the building of 3D views of the internal structure of the printed specimens. The resolution of radiographic imaging is 1920 × 1536 pixels. More than 1440 2D radiographic images are needed to build the tomograms (3D images). The voxel (pixel in 3D) size varied between 30 µm and 39 µm. From 15 to 20 minutes per sample are needed to accomplish the scanning. Stacks of the 3D microstructures of the printed ABS are reconstructed using the filtered back-projection method using the X-Act software from Rx-Solutions. The image size totalizes 1.20 to 1.24 billon voxels for undeformed samples and 0.67 to 0.93 billion voxels for the deformed ones. The volumes concerned are typically $(31 \times 32 \times 33)$ mm^3 for the undeformed samples and $(44 \times 51 \times 17)$ mm^3 for the deformed ones. Image processing is conducted to isolate the features of interest using ImageJ free software.

Finite element computation

Finite Element (FE) model based on COMSOL multi-physics software is developed to study the damage kinetics in printed ABS samples under compression conditions. The model uses an intuitive 2D geometry that represents slices within the printed structure. The in-plane configuration (XY) is

considered as it represents all possible configurations of filament arrangement according to the printing angle θ. The geometry and the definition of filament crossing within Comsol software are illustrated in Figure 3. The geometry corresponds to a two-layer sequence on which an array of crossed filaments draw a regular raster that alternate stiff square cells and weak interphases.
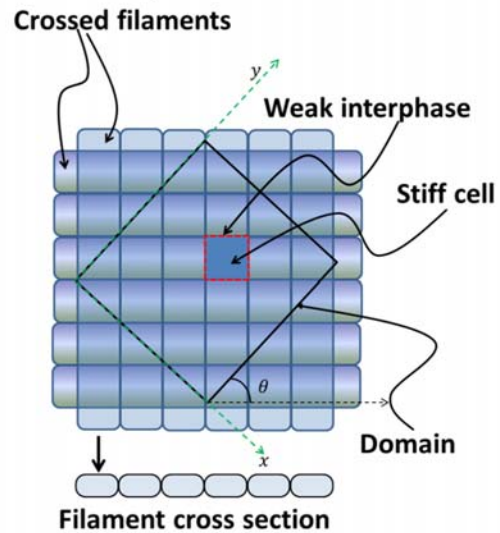

Figure 3. Definition of the 2D computational domain that alternates stiff and weak regions according to the filament sequences in the printed structure.

These interphases are filament junctions of a low cohesive structure. The weak structure represents the effect of the porous network generated during processing. The stiffness within the computation domain can be described using the scaling law

$$E(m(x,y)) = \begin{cases} E_{ABS} & if \ m \notin \partial\Gamma \\ \alpha \times E_{ABS} \times D(\varepsilon_i) & if \ m \in \partial\Gamma \end{cases} \quad (1)$$

where E_{ABS} is the filament Young's modulus of the as-received ABS wires ($E_{ABS} = 1.36$ GPa), α is a constant identified from experimental trends, $\partial\Gamma$ is the junction region, $m(x,y)$ is a material point from the computation domain, ε_i is a strain expression, D is a damage variable related to the stiffness loss. The following damage law is proposed based on a sigmoid form

$$D = 1 - \frac{\beta}{1+e^{-\gamma(\varepsilon_i - \varepsilon_0)}} \quad (2)$$

Subject to

$$\varepsilon_i =$$

$$\sqrt{\left(\varepsilon_{11}(x,y)\right)^2 + \left(\varepsilon_{22}(x,y)\right)^2 + \left(\varepsilon_{12}(x,y)\right)^2}|\varepsilon_{11} >$$

$$0; \varepsilon_{22} > 0 \tag{3}$$

where $\beta, \gamma, \varepsilon_0$ are parameters of the damage kinetics to be identified from the experiment.
The material properties of both the stiff and weak regions are considered isotropic. The domain orientation is adjusted according to the filament sequence generated by the printing angle θ. The generated elasticity maps are illustrated in Figure 4 for two different printing angles θ.
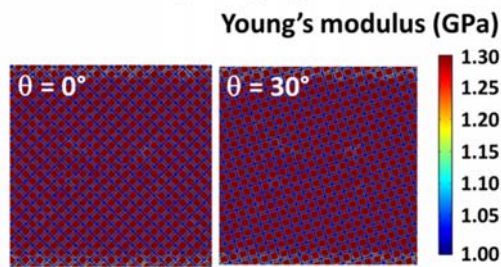

Figure 4. Young's modulus map associated to the 2D computational domain that alternates stiff and weak regions for two printing angles.

It is assumed that the damageable junction remain elastic during the simulation of compression loading. All computations are performed using Comsol® software. Irregular meshing is considered using plane triangular elements for compression stages. Regular meshing is considered for the printed sample using square elements (Figure 5).
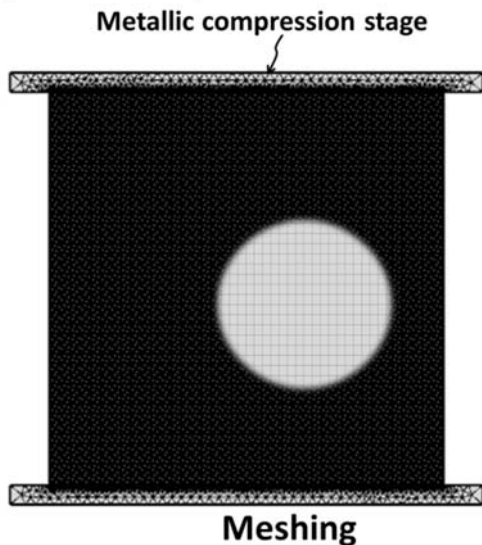

Figure 5. Meshing considered to simulate the compression of 3D printed structure.

The model contains 2.70×10^6 dof (degrees of freedom). Boundary conditions correspond to a constrained displacement in Y-direction for nodes of the bottom line (Y = 0), and uniform displacement for nodes from the opposite edge at Y= 1.

Experimental Results

Figure 6 illustrates the compression sequences for all tested conditions ($\theta=0°$, $\theta=30°$, $\theta=45°$, $\theta=60°$).
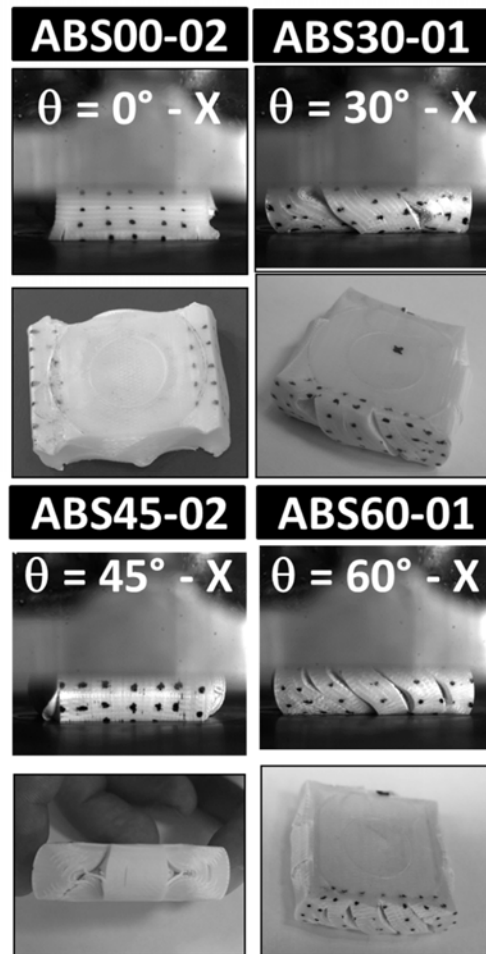

Figure 6. Sequence of compression of 3D printed ABS as a function of the printing angle.

The visual examination of the compressed specimens well show damages in the form of filament decohesion that follow different paths according to the filament sequences. This type of behavior is highly reproducible according to various replicates used during the testing campaign (less than 1% of mismatch in the area under the curves). The comparison between the mechanical responses in

Figure 7 demonstrates significant differences between the printed structures. The examination of the load response in lateral direction show distinct features for the printing angle of 0° in the load interval (20, 50) %. The observed response is affected by damage during the plasticity stage compared to the other printing angles. This damage is related to the development of macrocracks, filament decohesion and shearing bands. The force drop within the plasticity stage is due to this significant shearing that takes place only for θ= 0°.
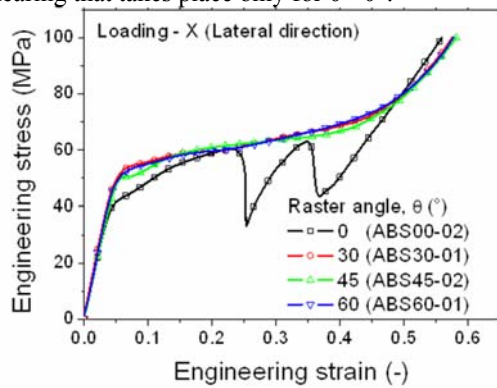

Figure 7. Compression response of the 3D printed structures showing differences in damage behavior depending on the printing angle.

Simulation Results

In order to provide an explanation of the observed damages, which are only characteristics of the printing angle 0°, finite element results are considered in Figure 8.
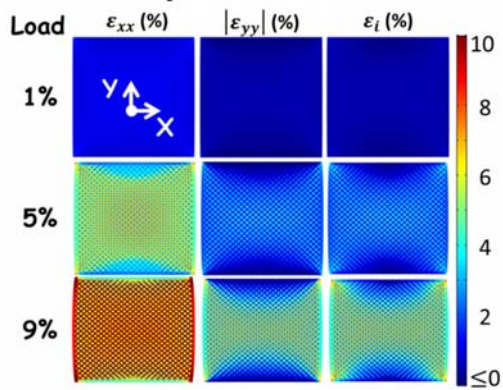

Figure 8. Finite element results showing the development of compression and tension fields for a 3D printed structure with the printing angle θ=0°. Three components of the strain field are illustrated for an increasing load level.

The simulations performed on the cross-section views in XY demonstrate the effect of filament crossing in the plane of construction (XY) where the lack of cohesion between filaments induce, for the printing angle θ=0°, a positive strain field due to the Poisson's expansion. A compressive strain field remains the main characteristic of the deformation field especially close to the compression stages. The considered FE model is capable of capturing the damage evolution thanks to the criterion implemented in equations 2 and 3. This damage triggers the regions of large positive strain as the ones connecting the weak regions at the filament junctions. It is clear that the damage connects more substantially as there is limited effect of the compression field. All regions of positive stress percolate in the lateral directions, which explain the severe damage development and force drop observed in Figure 7. To illustrate better the effect of printing angle on the development of damage, all strain fields are compared in Figure 9 for all considered printing angles.
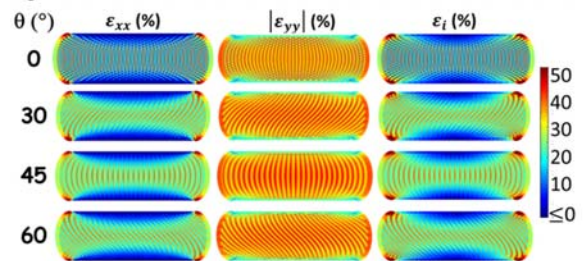

Figure 9. Compression between the strain fields for all printing configurations.

For the case of the printing angle θ = 0°, preferential damage sites are predicted at the corners (largest levels of strain component ε_{yy}). Damage develops to form shear bands because of the alternation of positive and negative stresses. The strain variation allows a significant level of mode II propagation along the boundary. It also excludes the inner part close to the compression stage because of the prevailing compression field.

For all other printing angles, the extension of damage from the outer to the inner part is stopped by the compression field that develops at the center of the specimen. Thus, the predicted strain field suggests that no pore opening mechanism is possible to drive significant damage. As a consequence, there is no force drop observed during the plasticity stage (Figure 7). These predictions are supported by the X-ray micro-tomography analysis of the deformed structures as shown in Figure 10. As can be seen, for the printing angle 0°, the damage percolation in all space directions is significant and can be related to the predicted positive strain that develops during the Poisson's expansion. Figure 10 shows a significant band shearing that connects all micro-cracks in the

lateral directions. For the case of the printing angle 30°, a significant deviation of the damage towards compression fields do not allow a large percolation and only limited damage as the one predicted in Figure 9 prevails. This is also the case for the remaining printing angles.
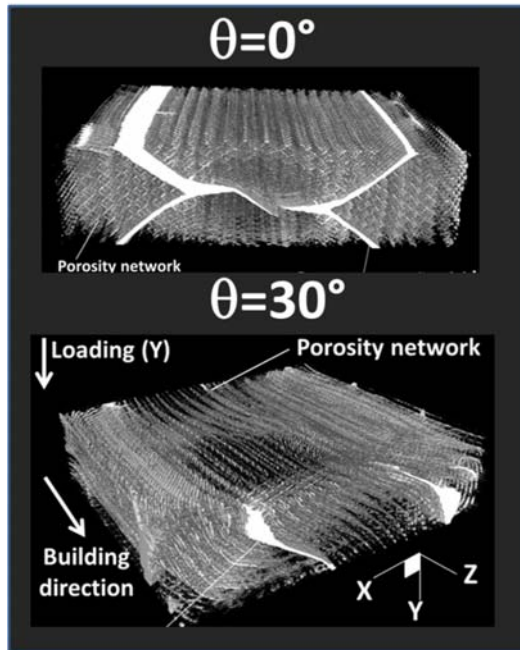

Figure 10. Evidence of damage percolation provided by X-ray micro-tomography imaging.

Conclusions

The simulation of the filament arrangement proved to be the best strategy to demonstrate the role of the process-induced porosity by means of a damage model that takes into account the underlined microstructure in 3D printed features.
As a conclusion, damage extension can be considered as exclusively related to the ability to connect porosities generated by the FDM process along particular paths. In the case of the printing angle of 0°, the Poisson's expansion allows pore connectivity to drive the failure of the material because the filaments are arranged in a way to a allow a strong percolation and limited effect of the compression field. The finite element results demonstrate that damage connectivity along the diagonals of the 3D printed ABS is assisted by shearing mode and pore percolation. This mechanism is not strong enough to allow the same percolation for the remaining printing angles because damage extension is arrested by the compression field.

References

1. Yan X and Gu P.A review of rapid prototyping technologies and systems. *Computer-Aided Design*,**28**(4),307-318(1996).
2. Wong KV and Hernandez A.A Review of Additive Manufacturing. *ISRN Mechanical Engineering*,**2012**,1-10(2012).
3. Pham DT and Gault RS.A comparison of rapid prototyping technologies. *International Journal of Machine Tools & Manufacture*,**38**(10-11),1257-1287(1998).
4. Ventola CL.Medical Applications for 3D Printing: Current and Projected Uses. *Pharmacy and Therapeutics*,**39**(10),704-711(2014).
5. Uriondo A, Esperon-Miguez M, and Perinpanayagam S.The present and future of additive manufacturing in the aerospace sector: A review of important aspects. *P I Mech Eng G-J Aer*,**229**(11),2132-2147(2014).
6. Giffi CA, Gangula B, and Illinda P. 3D opportunity in the automotive industry. Additive manufacturing hits the road: Deloitte University Press, 2014. pp. 24.
7. Gibson I, Kvan T, and Ming LW.Rapid prototyping for architectural models. *Rapid Prototyping J*,**8**(2),91-99(2002).
8. Lipton JI, Cutler M, Nigi F, Cohen D, and Lipson H.Additive manufacturing for the food industry. *Trends Food Sci Tech*,**43**(1),114-123(2015).
9. Peng AH, Xiao XM, and Yue R.Process parameter optimization for fused deposition modeling using response surface methodology combined with fuzzy inference system. *Int J Adv Manuf Tech*,**73**(1-4),87-100(2014).
10. Croccolo D, De Agostinis M, and Olmi G.Experimental characterization and analytical modelling of the mechanical behaviour of fused deposition processed parts made of ABS-M30. *Comp Mater Sci*,**79**,506-518(2013).
11. Tymrak BM, Kreiger M, and Pearce JM.Mechanical properties of components fabricated with open-source 3-D printers under realistic environmental conditions. *Mater Design*,**58**,242-246(2014).
12. Smith WC and Dean RW.Structural characteristics of fused deposition modeling polycarbonate material. *Polym Test*,**32**(8),1306-1312(2013).

13. Ben Hassana O, Guessasma S, Belhabib S, and Nouri H.Explaining the Difference Between Real Part and Virtual Design of 3D Printed Porous Polymer at the Microstructural Level. *Macromolecular Materials and Engineering* (2016).

14. Guessasma S, Belhabib S, and Nouri H.Significance of pore percolation to drive anisotropic effects of 3D printed polymers revealed with X-ray μ-tomography and finite element computation. *Polymer*,**81**,29-36(2015).

15. Guessasma S, Zhang W, Zhu J, Belhabib S, and Nouri H.Challenges of additive manufacturing technologies from an optimisation perspective. *International Journal for Simulation and Multidisciplinary Design Optimization*,**6**,A9(2016).